



HAL
open science

The mineralocorticoid receptor modulates timing and location of genomic binding by glucocorticoid receptor in response to synthetic glucocorticoids in keratinocytes

Elena Carceller-Zazo, Lisa Sevilla, Omar Pons-Alonso, Álvaro Chiner-Oms, Larbi Amazit, Thi an Vu, Géraldine Vitellius, Say Viengchareun, Iñaki Comas, Yan Jaszczyszyn, et al.

► To cite this version:

Elena Carceller-Zazo, Lisa Sevilla, Omar Pons-Alonso, Álvaro Chiner-Oms, Larbi Amazit, et al.. The mineralocorticoid receptor modulates timing and location of genomic binding by glucocorticoid receptor in response to synthetic glucocorticoids in keratinocytes. *FASEB Journal*, 2022, 37 (1), pp.e22709. 10.1096/fj.202201199RR . hal-04292010

HAL Id: hal-04292010

<https://hal.science/hal-04292010v1>

Submitted on 28 Nov 2024

HAL is a multi-disciplinary open access archive for the deposit and dissemination of scientific research documents, whether they are published or not. The documents may come from teaching and research institutions in France or abroad, or from public or private research centers.

L'archive ouverte pluridisciplinaire **HAL**, est destinée au dépôt et à la diffusion de documents scientifiques de niveau recherche, publiés ou non, émanant des établissements d'enseignement et de recherche français ou étrangers, des laboratoires publics ou privés.

RESEARCH ARTICLE

The mineralocorticoid receptor modulates timing and location of genomic binding by glucocorticoid receptor in response to synthetic glucocorticoids in keratinocytes

Elena Carceller-Zazo¹ | Lisa M. Sevilla² | Omar Pons-Alonso² | Álvaro Chiner-Oms³ | Larbi Amazit^{1,4} | Thi An Vu¹ | Géraldine Vitellius¹ | Say Viengchareun¹ | Iñaki Comas³ | Yan Jaszczyszyn⁵ | Montserrat Abella^{6,7} | Andrea Alegre-Martí^{6,7} | Eva Estébanez-Perpiñá^{6,7} | Marc Lombès¹ | Paloma Pérez² 

¹Inserm, Physiologie et Physiopathologie Endocrinienne, Université Paris-Saclay, Le Kremlin-Bicêtre, France

²Department of Pathology and Molecular and Cell Therapy, Instituto de Biomedicina de Valencia (IBV-CSIC), Valencia, Spain

³Department of Genomics and Proteomics, Instituto de Biomedicina de Valencia (IBV-CSIC), Valencia, Spain

⁴Unité Mixte de Service UMS-44, Le Kremlin Bicêtre, France

⁵CEA, CNRS, Institute for Integrative Biology of the Cell, Université Paris-Saclay, Gif-sur-Yvette, France

⁶Structural Biology of Nuclear Receptors, Department of Biochemistry and Molecular Biomedicine, Faculty of Biology, University of Barcelona, Barcelona, Spain

⁷Institute of Biomedicine of the University of Barcelona (IBUB), University of Barcelona, Barcelona, Spain

Correspondence

Paloma Pérez, Instituto de Biomedicina de Valencia (IBV-CSIC), Jaime Roig 11, Valencia 46010, Spain.

Email: pperez@ibv.csic.es

Marc Lombès, Inserm U1185, Faculté de Médecine Paris-Saclay, 63 Rue Gabriel Péri, Le Kremlin-Bicêtre Cedex 94276, France.

Email: marc.lombes@universite-paris-saclay.fr

Funding information

Institut National de la Santé et de la Recherche Médicale (Inserm); Ministerio de Ciencia e Innovación (MICINN), Grant/Award Number: PID2020-114652RB-I00 and PDC2021-121688-I00

Abstract

Glucocorticoids (GCs) exert potent antiproliferative and anti-inflammatory properties, explaining their therapeutic efficacy for skin diseases. GCs act by binding to the GC receptor (GR) and the mineralocorticoid receptor (MR), co-expressed in classical and non-classical targets including keratinocytes. Using knockout mice, we previously demonstrated that GR and MR exert essential nonoverlapping functions in skin homeostasis. These closely related receptors may homo- or heterodimerize to regulate transcription, and theoretically bind identical GC-response elements (GRE). We assessed the contribution of MR to GR genomic binding and the transcriptional response to the synthetic GC dexamethasone (Dex) using control (CO) and MR knockout (MR^{EKO}) keratinocytes. GR chromatin immunoprecipitation (ChIP)-seq identified peaks common and unique to both genotypes upon Dex treatment (1 h). GREs, AP-1, TEAD, and p53 motifs were enriched in CO and MR^{EKO} peaks. However, GR genomic binding was 35% reduced in MR^{EKO}, with

Abbreviations: ChIP-seq, Chromatin immunoprecipitation sequencing; CO, control; CORT, corticosterone; DBD, DNA-binding domain; Dex, dexamethasone; GCs, glucocorticoids; GR, glucocorticoid receptor; GRE, GC-response element; LBD, ligand-binding domain; MR, mineralocorticoid receptor; MREKO, MR epidermal knockout; SPR, surface plasmon resonance.

Elena Carceller-Zazo and Lisa M. Sevilla contributed equally to this work as first authors.

Marc Lombès and Paloma Pérez contributed equally to this work as senior authors.

This is an open access article under the terms of the [Creative Commons Attribution-NonCommercial-NoDerivs](https://creativecommons.org/licenses/by-nc-nd/4.0/) License, which permits use and distribution in any medium, provided the original work is properly cited, the use is non-commercial and no modifications or adaptations are made.

© 2022 The Authors. *The FASEB Journal* published by Wiley Periodicals LLC on behalf of Federation of American Societies for Experimental Biology.

significantly decreased GRE enrichment, and reduced nuclear GR. Surface plasmon resonance determined steady state affinity constants, suggesting preferred dimer formation as MR-MR > GR-MR ~ GR-GR; however, kinetic studies demonstrated that GR-containing dimers had the longest lifetimes. Despite GR-binding differences, RNA-seq identified largely similar subsets of differentially expressed genes in both genotypes upon Dex treatment (3 h). However, time-course experiments showed gene-dependent differences in the magnitude of expression, which correlated with earlier and more pronounced GR binding to GRE sites unique to CO including near *Nr3c1*. Our data show that endogenous MR has an impact on the kinetics and differential genomic binding of GR, affecting the time-course, specificity, and magnitude of GC transcriptional responses in keratinocytes.

KEYWORDS

epidermal keratinocytes, genomic binding, glucocorticoid and mineralocorticoid receptors, glucocorticoids, transcription

1 | INTRODUCTION

Glucocorticoids (GCs) have been prescribed to treat chronic inflammatory conditions, including the prevalent skin diseases atopic dermatitis (AD) and psoriasis, for more than 60 years due to their potent anti-inflammatory properties. However, continuous treatment or high doses of GCs often lead to unwanted systemic side effects, including hypertension, osteoporosis, adrenal insufficiency, cataracts, glaucoma, diabetes, skin atrophy, and delayed wound healing.^{1–5} Also, GC treatments elicit highly variable outcomes among patients due to differences in sensitivity to these ligands,⁶ underscoring the need to understand the cell type- and context-specific actions to optimize current therapies.^{2,3}

GCs act through a dual system formed by the corticosteroid receptors GC receptor (GR/*NR3C1*) and mineralocorticoid receptor (MR/*NR3C2*), members of the steroid subclass of nuclear receptors that, upon hormone binding, act as ligand-activated transcription factors (TFs).^{5,7,8} GR and MR comprise four structural and functional domains: an N-terminal domain, a DNA-binding domain (DBD), a flexible hinge region, and a ligand-binding domain (LBD). Upon GC binding, GR and MR dissociate from multimeric cytoplasmic chaperone complexes, undergo posttranslational modifications, and translocate to the nuclear compartment, where they regulate gene expression through DNA-binding-dependent and -independent mechanisms.^{3,9,10}

GR and MR are highly similar in structure and function, with 94% amino acid identity in their DBDs, implying that, theoretically, both can recognize identical consensus DNA sequences known as GC response elements (GRE; AGAACAnnnTGTTCT). While this would result in transcriptional regulation of the same target genes, GR and MR differ in the cell-type expression pattern and affinity

for endogenous ligands. GR expression is ubiquitous and activated only by GCs; in turn, MR shows a more restricted expression pattern and can bind GCs and the mineralocorticoid aldosterone with similar affinity. Also, the differential expression of 11 β -hydroxysteroid dehydrogenase (HSD11B) type I and II enzymes, which catalyze the interconversion between active and inactive GCs, respectively, modulates the tissue-specific availability of active hormone, and therefore, the specific activation of these corticosteroid receptors.⁸

GR and MR can also promote or suppress gene transcription indirectly by interfering with other TFs (typically AP-1 or NF- κ B) bound to their respective DNA-binding sites.^{3,5,11,12} GR but not MR can also repress inflammatory genes by binding to negative (n)GREs preventing the assembly of an active transcription complex, or to unrelated sequences called inverted repeat (IR)nGREs, to which it is recruited along with corepressors.^{5,13} Also, both GR and MR can interfere with signal transduction components such as MAPKs or PI3 kinases. However, and in contrast to GR, typically anti-inflammatory, MR can act as pro- or anti-inflammatory depending on the cell type and the ligand.¹⁴

The role of MR in mediating GC effects has been long disregarded despite the fact that endogenous GCs bind to MR with 10-fold higher affinity than GR. However, in recent years, there is accumulating evidence that GR-MR cross-talk and heterodimer formation modulate the specificity and magnitude of the GC-regulated transcriptional responses.^{15–29}

In cells with co-expression of both receptors, transcriptional outcome will depend on ligand availability, the GR:MR relative ratio, formation of homo- or heterodimers, patterns and kinetics of GR- and MR- genomic binding, and selective GR-MR interactions with cell type-specific

TFs and co-regulators.^{15,23,24,30,31} Recently, MR was shown to tether to genomic DNA by GR in neuroblastoma cells, contributing to an augmented GC transcriptional response.¹⁶ Moreover, studies revealed that genomic binding of distinct MR- and GR- homo- and heterodimers in response to GCs or aldosterone in a human renal cell line followed different kinetics.²³

The skin, given its anatomical location and continuous exposure to chemical and mechanical injuries, such as UV radiation, microorganisms, and wounding, is a frequent target of inflammatory diseases.³² Among the different cutaneous compartments, the epidermis is mainly formed by keratinocytes and constitutes the outer epithelial barrier, crucial to modulate cutaneous immunity and host defense and to protect the organism from external damage.³² Keratinocytes only proliferate in the epidermal basal layer, then migrate outward and differentiate forming squames that together with cross-linked lipids form the outmost layer, the stratum corneum. Perturbations of the skin barrier favor alterations in symbiotic host-microbiota relationship and associated immune responses, and are the bases of many inflammatory cutaneous disorders.^{33,34}

In previous studies, we demonstrated that epidermal GR and MR play key roles in the development, aging, and homeostasis of skin via nonoverlapping functions, suggesting biologically relevant cross-talk.³⁵ By proximity ligation assays, we identified GR-MR heterodimers in mouse keratinocytes, both in the cytoplasm (in the absence of the synthetic ligand dexamethasone, Dex), and in the nucleus upon Dex treatment.²⁴ These interactions were functionally relevant as keratinocyte-specific loss of GR, MR, or both, decreased Dex-induced GRE-luciferase activity to different extents.^{24,36} While Dex response was absolutely dependent on the presence of GR, it decreased around 40% in MR epidermal KO keratinocytes (MR^{EKO}) relative to controls (CO) despite the fact that overall GR levels were similar in both genotypes.³⁶ However, the role of MR in modulating GR genomic binding and on transcriptional responses to GCs in keratinocytes is unknown.

To address these questions, we performed ChIP-seq and RNA-seq studies in CO and MR^{EKO} keratinocytes upon Dex treatment, and identified genomic targets of GR and associated changes in the transcriptome. MR-deficient keratinocytes showed a significant reduction of GR peaks relative to CO (35%). While AP-1, GRE, TEAD, and p53 motifs were found to be overrepresented in both CO and MR^{EKO} ChIP-seq datasets, there were statistically significant differences in signal intensity between genotypes. Along these lines, there was a decrease in GRE motifs in GR-bound sequences (GBS) in MR^{EKO} versus CO cells. Immunofluorescence and nuclear fractionation experiments indicated that GR showed a decreased nuclear localization in response to

Dex in MR^{EKO} versus CO. Also, using surface plasmon resonance (SPR), we assessed GR- and MR- protein-protein interactions and estimated the affinity and kinetics of their physical associations. Data suggest that MR homodimers have the highest affinity but the shortest lifetime, while GR homodimers and GR/MR heterodimers show similar intermediate affinity and extended dimer half-life.

Despite differential patterns in GR nuclear localization and DNA recruitment in the presence or absence of MR, the gene expression profiles in response to 3 h of Dex treatment were very similar in CO and MR^{EKO}. However, kinetics studies demonstrated good correlation between earlier and more pronounced GR binding to GBS with GRE sites unique to CO near *Nfil3* and *Nr3c1*, and transcript levels.

2 | MATERIAL AND METHODS

2.1 | Cell culture

Immortalized mouse control (CO) and MR epidermal KO (MR^{EKO}) keratinocyte cell lines were generated as described from 8-week-old female mouse dorsal skin.³⁷ Keratinocytes were isolated following overnight incubation of skin with 0.25% trypsin-PBS at 4°C and cultured on mitomycin C-treated J2-3T3 feeders in type I collagen (Gibco)-coated flasks with DMEM (Gibco)-Ham's F12 (Biowest) (3:1) medium supplemented with 0.18 mM adenine, 0.35 mM calcium, 7.5% FBS (Biowest), 100 U/ml penicillin/100 µg/ml streptomycin (Biowest), 2 mM glutamine (Biowest), 0.25 µg/ml amphotericin B (Biowest), 5 µg/mL insulin (Sigma), 0.1 nM cholera toxin (Sigma), and 10 ng/ml EGF (Peprotech). Following eight passages, spontaneously immortalized lines arose.³⁶ The MR^{EKO} cell line showed no significant differences in GR protein or mRNA expression, relative to CO.^{24,36}

To evaluate response to dexamethasone (Dex, 100 nM; Sigma) or corticosterone (CORT, 100 nM; Sigma) treatment, keratinocytes were cultured in type I collagen-coated dishes in the absence of feeders. The MR antagonist eplerenone was used at 10 µM (Sigma). Forty-eight hours prior to experimentation, cells were washed twice with PBS and incubated with the medium described above, with FBS replaced by 7.5% dextran-coated charcoal (Sigma)-stripped serum for steroid starvation.

2.2 | ChIP-sequencing

Steroid-starved CO and MR^{EKO} keratinocytes were treated with vehicle (EtOH) or 100 nM Dex for 1 h prior to processing. The iDeal ChIP-Seq kit for Transcription Factors (Diagenode, Seraing, Belgium), was used for

sample preparation. Chromatin shearing was performed by sonication with Bioruptor Pico (Diagenode) for 10 min (30"ON/30"OFF cycles). A total of 5 µg of GR-specific antibody (sc-393232X, Santa Cruz Biotechnology) were used for immunoprecipitation. Input controls were 1% chromatin used for ChIP. ChIP-qPCR experiments were performed as previously described,³⁸ with 3 µg of antibody and Dynabeads™ Protein A or G magnetic beads (Invitrogen). For MR ChIP, 4 µg of MR-specific antibody (21854-1-AP, Proteintech) was used.

ChIP samples and respective input controls (inputs for CO or MR^{EKO} Vehicle were used to normalize both treatment conditions within respective genotype) were processed for library construction and Illumina sequencing in the NGS Core Facility of the Institute for Integrative Biology of the Cell (<http://www.i2bc.paris-saclay.fr/>). DNA fragments were end repaired and dA-tailed with the NEBNext® Ultra™ II End Repair/dA-Tailing Module and Illumina TruSeq adapters were ligated with the NEBNext® Quick Ligation Module (New England Biolabs Inc.). Libraries were amplified with Kapa Biosystems Hifi polymerase (Sigma). Library quality was verified on an Agilent Bioanalyzer 2100, using an Agilent High Sensitivity DNA Kit. Libraries were pooled in equimolar proportions and sequenced on a Paired-End 2×43 bp run, on the Illumina NextSeq500.

Raw sequence reads were quality checked, adapter trimmed, and filtered using Cutadapt1.15 and FastQC v0.11.5 and only reads longer than 10 bp were kept for analysis. Trimmed sequences were mapped to the *Mus musculus* genome (assembly: GRCm38/mm10) using the bwa-mem algorithm. Only reads mapped with a mapping quality of 60 (maximum) were kept for further analyses. Peak calling and search for enrichment of TF-binding motifs in identified GR-bound sequences (GBS) were performed using HOMER,³⁹ with the findPeaks and findMotifsGenome functions, using respective input controls for each genotype. Peaks were assigned an identification code based on genomic location for comparative purposes. Overlapping intervals were grouped into "active regions," defined by the start coordinate of the most upstream interval and the end coordinate of the most downstream interval.⁴⁰ The criterion for overlapping represents at least 50% coincidence among peak sequences. Peaks were visualized using Integrated Genomics Viewer (version 2.11.9) Software.⁴¹ We used CREMA (Cis-Regulatory Element Motif Activities; <https://crema.unibas.ch/cruma.ra/>) to identify statistically significant differences in TF motif enrichment in identified CO and MR^{EKO} GBS. Comprehensive motif analysis with XTREME⁴² determined consensus GRE sequences and the positional distribution in GBS, as well as the percentage of GBS in datasets containing one or more identified motifs (parameters:

motif width between 6 and 30 bp and any number of repetitions of motif within peaks). Gene ontology was determined using DAVID functional clustering with an EASE score less than 0.05 and medium stringency.^{43,44}

2.3 | RNA isolation, cDNA preparation, and qPCR

Total RNA was isolated using TRI reagent (Molecular Research Center, Inc., Euromedex, Mundolsheim, France). The RevertAid H Minus Reverse Transcriptase kit (ThermoFisher) was used to generate cDNA.

qPCR was performed with gene-specific oligonucleotides (0.3 µM each; Sigma) and the FastStart Universal SYBR Green Master mix ROX (Roche) with the Quant Studio 5 Real-Time PCR System (Applied Biosystems, Foster City, California, USA). In the case of cDNA amplification, Ct values were normalized to those of the housekeeping gene *Hprt1*. In the case of ChIP-qPCR, Ct values of each ChIP were normalized to those of respective inputs. Technical triplicates were used; and a minimum of three biological replicates per experimental group were assessed to calculate the mean value ± SD. Primer sequences are in Table S1 and unless otherwise indicated were designed using Primer-BLAST (NIH, <https://www.ncbi.nlm.nih.gov/tools/primer-blast/>). Primers from PrimerBank (<https://pga.mgh.harvard.edu/primerbank/>) are indicated with corresponding IDs.

2.4 | RNA sequencing

Steroid starved CO and MR^{EKO} keratinocytes were treated with vehicle (EtOH) or 100 nM Dex for 3 h prior to RNA isolation. This experiment was performed with two biological replicates per genotype and condition, which were subsequently pooled for library preparation and Illumina sequencing in the NGS Core Facility of the Institute for Integrative Biology of the Cell. Total RNA quality was assessed on an Agilent Bioanalyzer 2100, using RNA 6000 pico kit (Agilent Technologies). Directional RNA-Seq Libraries were constructed using the TruSeq total RNA Stranded library prep kit, with H/M/R Ribo-Zero reagents (Illumina). Quality of libraries was assessed on an Agilent Bioanalyzer 2100, using an Agilent High Sensitivity DNA Kit. Libraries were pooled in equimolar proportions and sequenced on a paired-end 51–35 bp run, with the Illumina NextSeq500.

FASTQ files were obtained from applying the bcl2fastq2 Conversion Software (V2.18.12) to the BCL files generated by the sequencer. Adapters were removed with Cutadapt 1.15; only reads longer than 10 bp were kept for analysis.

Filtered FASTQ files were mapped against the *Mus musculus* reference genome (assembly: GRCm38/mm10) with HISAT2, with the `-rna-strandness RF` argument. Absolute values ranging from 117 to 151 million paired-end 51–35 bp reads were obtained from samples.

Reads mapping on each feature were counted with the HTSeq-count script, with the “union” mode of overlapping and with the `—stranded` option for detecting reads falling in the reverse strand. A count table was created with the information derived from HTSeq-count for each sample. Later, the DESeq2 package in R was used to analyze differential gene expression using this count table as an input. The log₂ fold-change between the expression (normalized counts) of each gene in the Dex versus vehicle samples was calculated. With these values, we generated a distribution and identified outliers as $Q3 + 1.5 \cdot IQR$ and $Q2 - 1.5 \cdot IQR$. In addition, for each gene, we performed a Fisher test comparing the expression of both conditions, using the housekeeping gene *Hprt* as a normalization factor. The p-values obtained were adjusted using the Benjamini–Hochberg method.

2.5 | Nuclear fractionation

Steroid-starved CO and MR^{EKO} keratinocytes were treated with vehicle (EtOH) or 100 nM Dex for 1 h. Cells were lysed with hypotonic lysis buffer (10 mM HEPES pH 7.9, 10 mM KCl, 1 mM EDTA, 1 mM EGTA, 0.5 mM DTT, protease and phosphatase inhibitors). After incubation for 20 min on ice, IGEPAL was added to a final concentration of 0.05%. Cell lysates were centrifuged at 1000g for 10 min at 4°C to pellet nuclei. The supernatant (cytoplasmic fraction) was removed and nuclear proteins were extracted by incubating on ice for 45 min with lysis buffer (10 mM HEPES pH 7.9, 200 mM NaCl, 0.2 mM EDTA, 2 mM MgCl₂, 20% glycerol, 0.5 mM DTT, 0.1% IGEPAL, protease and phosphatase inhibitors), and centrifuged for 10 min at 16000g. The supernatant was the nuclear fraction. Protein concentrations were determined using Bradford reagent (Fisher).

2.6 | Immunoprecipitation and Immunoblotting

For immunoprecipitation of GR, equivalent quantities of nuclear extracts were diluted in IP buffer (50 mM Tris pH 7.6, 150 mM NaCl, 5 mM EDTA, 0.1% IGEPAL, protease and phosphatase inhibitors), precleared, and then incubated overnight at 4°C with 3 μg GR antibody (sc-393232). Protein G Dynabeads were added for 2 h at 4°C and then washed 3x with IP buffer; bound proteins were then eluted in Laemmli buffer.

Total nuclear extracts and immunoprecipitated proteins were separated on denaturing SDS-polyacrylamide gels and transferred to nitrocellulose (Amersham). Filters were probed overnight at 4°C using the following antibodies specific for: actin (A2066, Sigma), Pan-TEAD (13295, Cell Signaling), p63 (sc-8431, Santa Cruz), and GR (sc-1004, Santa Cruz). Following washing with TBS-Tween and incubation with anti-mouse or anti-rabbit HRP-linked secondary antibodies (NA931 and NA934, respectively, Cytiva, Merck), proteins were visualized using Pierce™ ECL Plus Western Blotting Substrate (Pierce, ThermoFisher) and the ImageQuant LAS 4000 mini Biomolecular Imager (GE Healthcare). Band intensities were quantitated using ImageJ software and normalized to Lamin A/C as loading control. Data (at least three biological replicates per group) are presented as mean ± SD.

2.7 | Immunofluorescence and high-throughput microscopy

After Dex treatment (100 nM) for indicated times, keratinocytes were fixed with 4% paraformaldehyde for 15 min at room temperature. After 15 min of permeabilization with 0.5% Triton X-100, cells were washed and incubated in blocking buffer (5% nonfat dry milk, 0.1% Tween20 in PBS) for 1 h. Then, the cells were incubated with GR-specific antibody (sc-393232X) overnight at 4°C. The next day, cells were washed five times and incubated with Alexa Fluor 555 conjugated anti-mouse secondary antibody (ThermoFisher). DAPI (Invitrogen) was used to stain nuclei. High-throughput microscopy was performed with an Arrayscan VTI microscope (ThermoFisher). For the quantification of the ratio of nuclear/cytoplasmic immunofluorescence (500–1500 individual cells per data group), we used the Molecular Translocation V4 BioApplication algorithm (vHCS Scan, version 6.3.1, Build 6586). Statistical significance was calculated using the nonparametric Kruskal–Wallis and the post hoc Dunn test (GraphPad software).

2.8 | Protein expression and surface plasmon resonance (SPR) analyses

Recombinant ancGR2-LBD cloned into a pMALCH10T vector was expressed as fusion protein with an N-terminal maltose-binding protein (MBP) and a hexahistidine (His) tag and purified to homogeneity using standard chromatographic procedures after cleavage with TEV protease.⁴⁵ Recombinant MR-LBD cloned into a pSMT3 vector was expressed as fusion protein with an N-terminal His-SUMO-tagged fusion protein and purified to homogeneity

using standard chromatographic procedures after cleavage with Ulp1 protease.⁴⁶

SPR analyses were performed at 25°C in a BIAcore T200 instrument (GE Healthcare). Highly purified, Dex-bound recombinant WT ancGR2-DBD-LBD, ancGR2-LBD, and MR-LBD were diluted in 10mM sodium acetate, pH 5.0, and directly immobilized on CM5 chips (GE Healthcare) by amine coupling at densities between 100 and 150 resonance units (RU). As a reference, one of the channels was also amine-activated and blocked in the absence of protein. The same protein samples were run over the ancGR2-LBD and MR-LBD immobilized partners in a running buffer including 50mM HEPES, pH 7.2, 50mM NaCl, 3% glycerol, 1mM dithiothreitol (DTT), 50µM Dex. *Nr3c1* (5'-GGATACACTGTGTACT-3'; 5'-AGTACACAGTGTATCC-3'), *Nfil3* (5'-TAGAACATTCTGTACT-3'; 5'-AGTACAGAATGTTCTA-3'), and *Tsc22d3* (5'-AAAAACAGAATGTTCA-3'; 5'-TGAACATTCTGTTT-3') oligonucleotides were run over the ancGR2-DBA-LBD immobilized partner in a pH 3 buffer consisting of 10mM HEPES, 150mM NaCl, 0.005% Tween-20, 10mM Na molybdate, and 5mM Zn citrate. Sensorgrams were analyzed with the BIAcore T200 Evaluation software 3.0 and fitted according to the Langmuir 1:1 model.

2.9 | Statistics and data analysis

Unless otherwise mentioned, statistical significance of experimental data was calculated using the GraphPad Prism software (version 5.2; GraphPad Software Inc., San Diego, CA) and IBM SPSS software. Data were obtained in at least three independent experiments. Data with normal distribution are presented as mean ± SD; non-normal data were reported as median ± interquartile range (Figure 2D) or mean ± SEM (Figure 3D). Means of two and three or more groups of normally distributed variables were compared by Student's t test or ANOVA with a Tukey post hoc test, respectively. The Mann-Whitney U test or the Kruskal-Wallis with a post hoc Dunn test was used to compare means of two and three or more groups, respectively, of non-normally distributed data. *p*-values <.05 were considered statistically significant. Biovenn was used to generate Venn diagrams.⁴⁷

3 | RESULTS

3.1 | Keratinocyte loss of MR reduces genomic GR recruitment in response to Dex

To assess whether GC-induced genomic GR binding could be altered by the absence of MR, CO, and MR^{EKO}

keratinocytes were treated with Dex (100nM) for 1 h followed by ChIP-seq. GR chromatin occupancy was mapped in the presence and absence of MR (Table S2). While identified GR-bound sequences (GBS) were only marginal in vehicle-treated CO and MR^{EKO} cells, Dex treatment dramatically increased GR chromatin occupancy in both genotypes (Table S2; Figure 1A). Importantly, the absence of MR correlated with an approximately 35% reduction in the number of GBS relative to CO (Figure 1A; 2761 vs 1829 peaks corresponding to 1804 vs 1242 genes, in CO and MR^{EKO}, respectively). Furthermore, in comparing the 1533 GBS common to both genotypes, an overall 10% decrease in tag counts was observed in MR^{EKO} versus CO (*p* < .0001).

To compare peaks and analyze overlap between CO and MR^{EKO} GBS, all peaks were assigned an identifier (Table S2). Then, overlapping intervals were grouped into "active regions," defined by the start coordinate of the most upstream interval and the end coordinate of the most downstream interval.⁴⁰ The criterion for overlapping represents at least 50% coincidence among peak sequences. Almost half (45%) of GBS identified in CO were not present in MR^{EKO}, indicating a striking dependence on MR for GR genomic binding (Figure 1B). In contrast, the majority of GBS (84%) identified in MR^{EKO} overlapped with those identified in CO (Figure 1B). However, multiple GBS were often detected *per* gene, some of which were common to both genotypes while others were unique for CO or MR^{EKO} (Table S2).

The identification of GBS in genes (nearest TSS) common to both genotypes (*Tsc22d3/Gilz* and *Per1*), unique to CO (*Nfil3*, *Nr3c1* and *Dusp10*), or unique to MR^{EKO} (*Hlf1* and *Lmnb2*) indicate context-dependent consequences of the loss of MR on GR binding (Figure 1C). Data were validated by ChIP-qPCR in independent experiments, showing reduction in GR binding to regulatory sequences of common (*Tsc22d3/Gilz1* and *Per1*) and unique (*Nfil3* and *Dusp10*) GBSs in MR^{EKO} versus CO (Figure 1D). Likewise, peaks unique to MR^{EKO} were also validated confirming increased GR binding relative to CO cells (Figure 1D; *Hlf* and *Lmnb2*). Moreover, treatment of CO cells with the MR antagonist eplerenone resulted in a reduction of GR recruitment to *Tsc22d3* and *Per1* of more than eight-fold (Figure S1). Altogether, these data indicate that MR plays a role in the Dex-induced GR genomic binding in keratinocytes.

Consistent with previous reports,^{48–50} after Dex treatment, most GBS in CO and MR^{EKO} keratinocytes were found in introns (46%–49%) and intergenic (36%–39%) regions while only 7%–8% of the peaks were found near promoters (Figure S2). Therefore, the absence of MR did not alter the genomic distribution of GR DNA-binding sites.

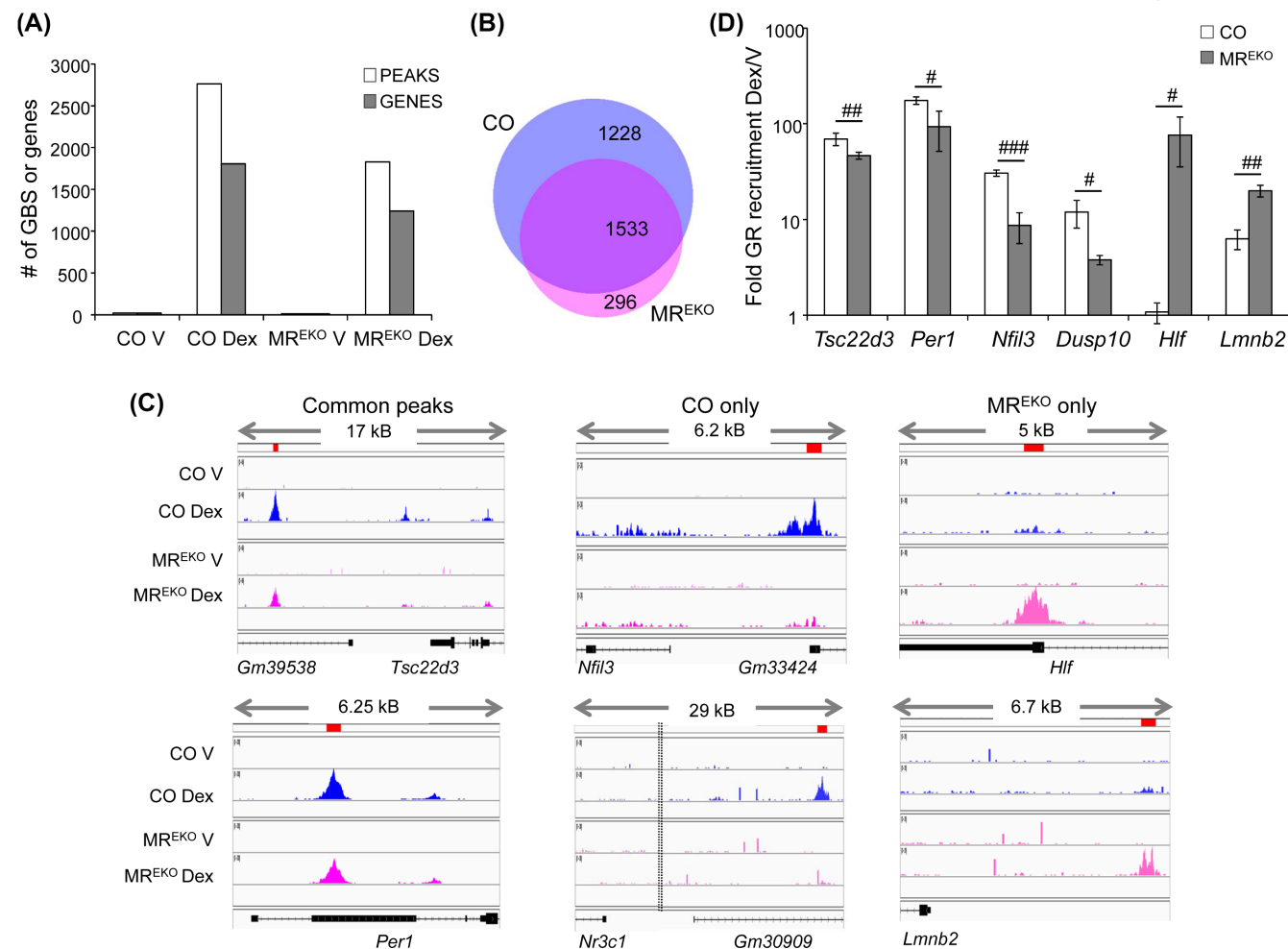


FIGURE 1 The lack of MR in keratinocytes correlates with an overall reduction in Dex-induced GR genomic recruitment. (A) GR genomic binding in control (CO) versus MR^{EKO} keratinocytes treated 1 h with either vehicle (V) or 100 nM Dex. The number of GR-bound sequences (GBS) and associated genes is indicated. (B) Venn diagram showing overlap of GBS identified in Dex-treated CO and MR^{EKO} cells. (C) Screenshots from IGV browser showing peaks common to both genotypes (*Tsc22d3/Gilz* and *Per1*), unique to CO (*Nfil3* and *Nr3c1*), and unique to MR^{EKO} (*Hlf* and *Lmn2*). Genomic regions corresponding to peaks are indicated by red bars. Dotted lines in screenshot of *Nr3c1* indicate break in X-axis genomic coordinates. (D) Validation by independent experiments of GR ChIP-qPCR for indicated genes; mean values and SD are shown. Hash symbols indicate statistically significant differences in recruitment between genotypes ($n = 3$; # $p < .05$; ## $p < .01$; ### $p < .001$).

To have direct evidence of MR binding to the identified GR-bound fragments, we performed MR-ChIP after treatment with Dex or the physiological ligand corticosterone (CORT) for 1 h. While Dex did not induce detectable MR binding to regulatory sequences such as *Nfil3*, *Nr3c1*, and *Dusp10* (not shown), CORT elicited robust MR binding to these sites as well as *Tsc22d3* and *Per1* (Figure S3). The fact that CORT also induced strong GR binding to the same regulatory sequences (Figure S3) indicate that, upon ligand binding, MR and GR can co-occupy DNA in these cells. However, the different magnitude of GR recruitment to distinct genomic sequences suggests that formation of GR/MR oligomers depends on genomic context.

3.2 | The absence of MR alters enrichment of GR-binding motifs, with significant decrease in GREs, and reduces GR nuclear localization

To determine the specific DNA sequences enriched within CO and MR^{EKO} GBS, we searched for TF-binding motifs in an unbiased manner using HOMER (Figure 2A). The top overrepresented motifs, common to both genotypes, included AP-1, GRE, TEAD, and p53. We used CREMA to determine whether there were statistically significant differences in TF motif enrichment between genotypes and found that importantly, GRE motifs were infra-represented in MR^{EKO} relative to

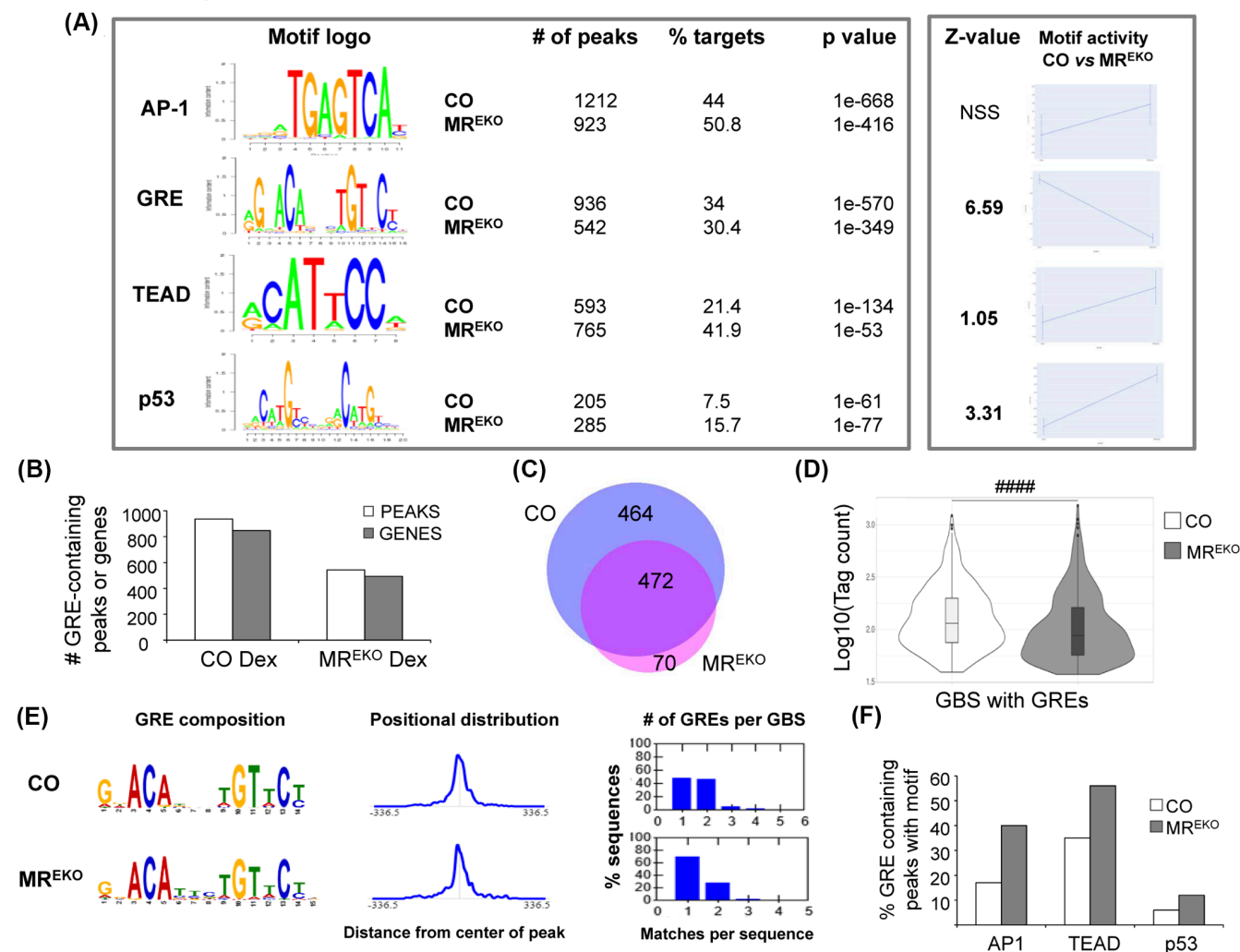


FIGURE 2 MR absence affects motif composition of GR-bound genomic regions and decreases GR binding to GRE-containing sequences. (A) Left panel: Transcription factor binding motif enrichment analysis was performed by HOMER. Motif logo of the top overrepresented motifs, number of peaks and percentage of targets containing motifs, and p-values, are indicated for each genotype. Right panel: Statistically significant differences in motif enrichment in CO versus MR^{EKO} (Z-value) determined by CREMA. Graphs represent changes in motif activity between genotypes. (B) Number of GRE-containing peaks and associated genes in CO versus MR^{EKO} Dex-treated cells. (C) Venn diagram depicting the overlap between GRE-containing GBS in CO and MR^{EKO}. (D) The plot shows the distribution of GRE tag counts for both genotypes represented by median values and interquartile range; $n = 472$; $#### p < 10^{-8}$. (E) XTREME results for palindromic GRE motifs identified in CO and MR^{EKO} datasets; left to right: sequence logo, positional distribution of motifs in GBS, and bar graphs showing percentage of GBS containing indicated number of GREs. (F) Percentages of indicated enriched TF motifs in the subsets of GRE-containing GBS in MR^{EKO} relative to CO cells.

CO, while TEAD and p53 motifs were overrepresented (Figure 2A).

The decreased number of peaks containing GREs in MR-deficient versus CO cells indicated that the GR affinity and/or specificity toward a subset of GRE motifs depend on the presence of MR (Figure 2B; 542 vs 936 peaks, respectively). Indeed, 47% of GRE-containing peaks were unique to CO (Figure 2C). Moreover, GBS with GREs identified in both genotypes showed a 14% decrease in tag count in MR^{EKO} versus CO (Figure 2D; p -value $< 10^{-8}$). Ontological analysis of GRE-containing peak-associated genes unique to CO showed enrichment in transcriptional regulation

and cell differentiation annotation clusters (Figure S4); notable genes within these categories included *Nfil3*, *Nr3c1*, *Dusp10*, *Nfkb1*, and *Pparg*. Comprehensive motif analysis of GBS by XTREME showed that the composition and positional distribution of palindromic GREs did not vary between genotypes. However, the number of GREs present in GR-bound genomic regions was decreased in MR^{EKO} versus CO datasets (Figure 2E). This suggests that MR is involved in cooperative interactions between multiple GRE within a GBS.

We evaluated the presence of identified enriched TF motifs (AP-1, TEAD, and p53) in the subsets of

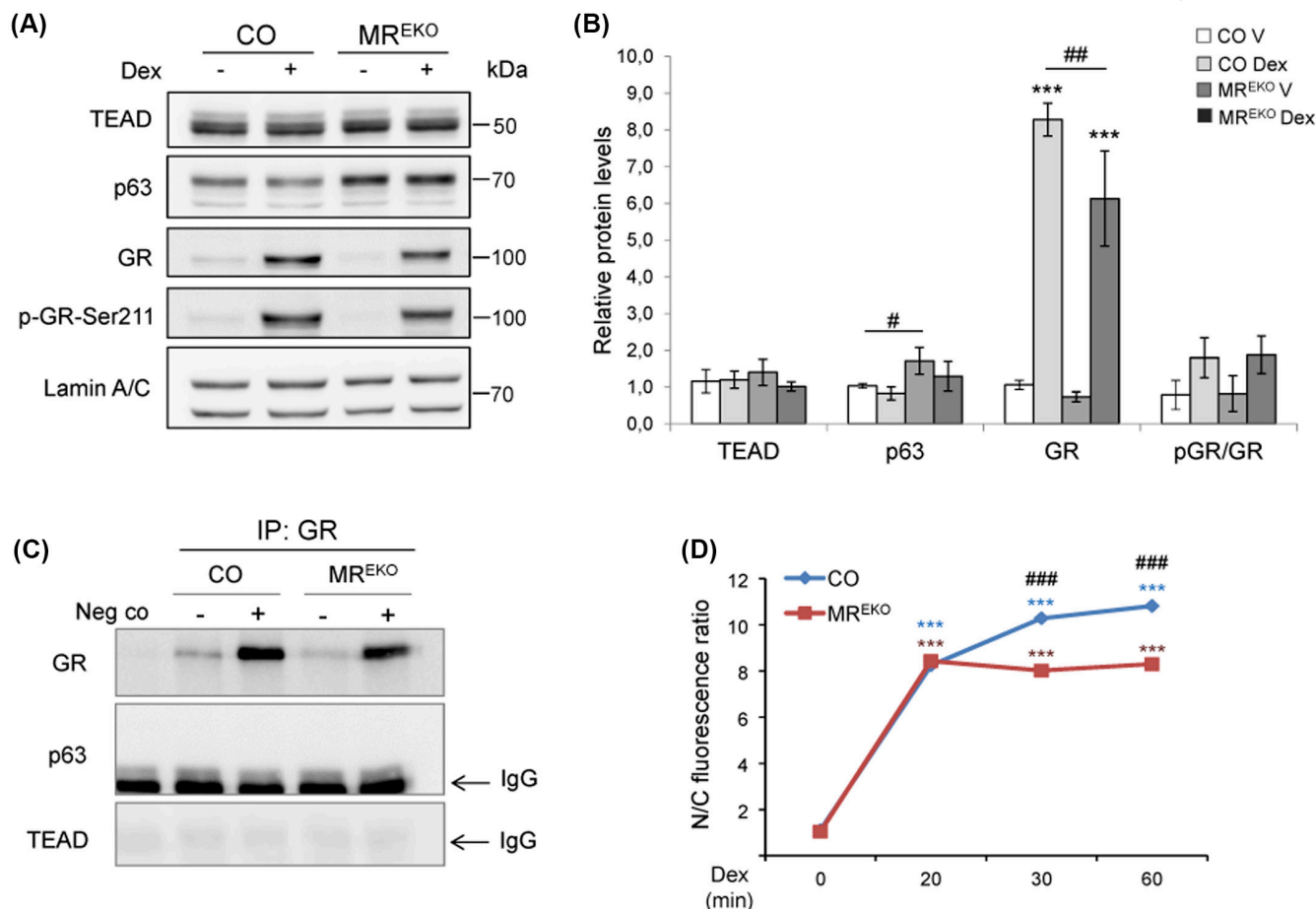


FIGURE 3 Nuclear GR, p63, and TEAD in CO and MR^{EKO} keratinocytes upon treatment with Dex. CO and MR^{EKO} keratinocytes were treated with vehicle or 100 nM Dex to evaluate the following parameters. (A) Expression and (B) quantitation of TEAD, p63, GR, and phospho(p)-GR, in CO and MR^{EKO} cells; Lamin A/C was used as reference for loading control. Mean values and SD are shown ($n = 4$; $^{\#}p < .05$; $^{\#\#}p < .01$; $^{***}p < .001$). (C) Immunoprecipitation studies to assess GR interaction with indicated TFs. (D) Nuclear/cytoplasmic (N/C) ratio of immunofluorescence for GR at indicated time points following treatment. Mean values and SEM are shown (a minimum of 500 individual cells per condition were quantitated; $n = 3$; *** , $^{###}p < .001$). Statistically significant differences relative to $t = 0$ are denoted by asterisks and those between genotypes by hash symbols.

GRE-containing GBS, and found increased co-occurrence with other motifs in MR^{EKO} relative to CO cells: TEAD (56% vs 35%), AP-1 (40% vs 17%), and p53 (12% vs 6%). These data suggest that these GBS may be maintained in the absence of MR due to interactions of GR with these TFs (Figure 2F).

While we did not detect any changes in the expression of TEAD between genotypes, the overrepresentation of p53 motifs correlated with constitutively increased expression of the epithelial-specific homolog of p53, p63 (Figure 3A,B). However, co-immunoprecipitation studies did not identify protein-protein interactions between GR and these TFs in the nucleus (Figure 3C).

To understand the mechanisms behind the decreased number of GRE-containing peaks in MR^{EKO} versus CO cells, we also assessed the expression and activity of GR. Following 1 h of Dex treatment, the levels of nuclear GR were significantly decreased in MR^{EKO} relative to CO

(by 25%), without changes in the ratio of phospho (p)-GRS211/total GR (Figure 3A,B). Next, we investigated the GR nuclear/cytoplasmic ratio at several time points following Dex treatment using immunofluorescence and high-throughput microscopy (Figure 3D). While at 20 min following treatment, CO and MR^{EKO} showed identical GR nuclear/cytoplasmic ratios, this ratio was significantly reduced in MR^{EKO} at 30 min (by 22%) and 1 h (by 23%).

3.3 | Dex-bound GR-LBD, MR-LBD self-associate, and GR-MR LBDs heterodimerize in solution

In cells that co-express GR and MR, the combinatorial of distinct homo- and heterodimers represents an important mechanism to modulate gene expression.²² After

expression and purification of GR-LBD and MR-LBD bound to Dex, we used surface plasmon resonance (SPR) to analyze the physical protein–protein interactions of the GR and MR homodimers as well as the suggested GR/MR heterodimers. The respective ligand-bound receptors were immobilized on sensor chips, and increasing concentrations of either ligand-bound protein were run over as analyte (Figure 4).

The analyses of SPR data demonstrated MR-LBD and GR-LBD self-association, showing steady state affinities (K_D) of $1.49 \pm 0.41 \mu\text{M}$ and $17.4 \pm 1.5 \mu\text{M}$, respectively (Figure 4A,C). Interestingly, the resulting K_D for MR homodimer was one order of magnitude lower than that obtained for GR homodimer. Also, the K_D of GR-LBD over MR-LBD was $11.6 \pm 1.5 \mu\text{M}$ (Figure 4B), suggesting that the order of preferred dimer formation ranks as MR-MR > GR-MR ~ GR-GR. However, kinetic studies demonstrated very different life time of respective dimers, with

MR homodimers showing the shortest $t_{1/2}$, followed by GR homodimers and GR/MR (Figure 4D–G).

Importantly, upon expression of GR multidomain (GR-DBD-LBD) protein, there was binding to specific regulatory sequences identified by ChIP-seq such as *Nr3c1*, *Nfil3*, and *Tsc22d3* (Figure S5). Note that the K_D for GR protein–DNA interactions was higher for the peaks unique to CO, *Nr3c1*, and *Nfil3*, relative to the common peak *Tsc22d3*, suggesting that MR contributes to GR binding to DNA.

3.4 | Dex transcriptional response in keratinocytes is largely mediated by GR and not MR

To analyze the contribution of MR in GR-mediated transcriptional responses to GCs, we treated CO and MR^{EKO} keratinocytes with 100 nM Dex or vehicle for 3 h, and

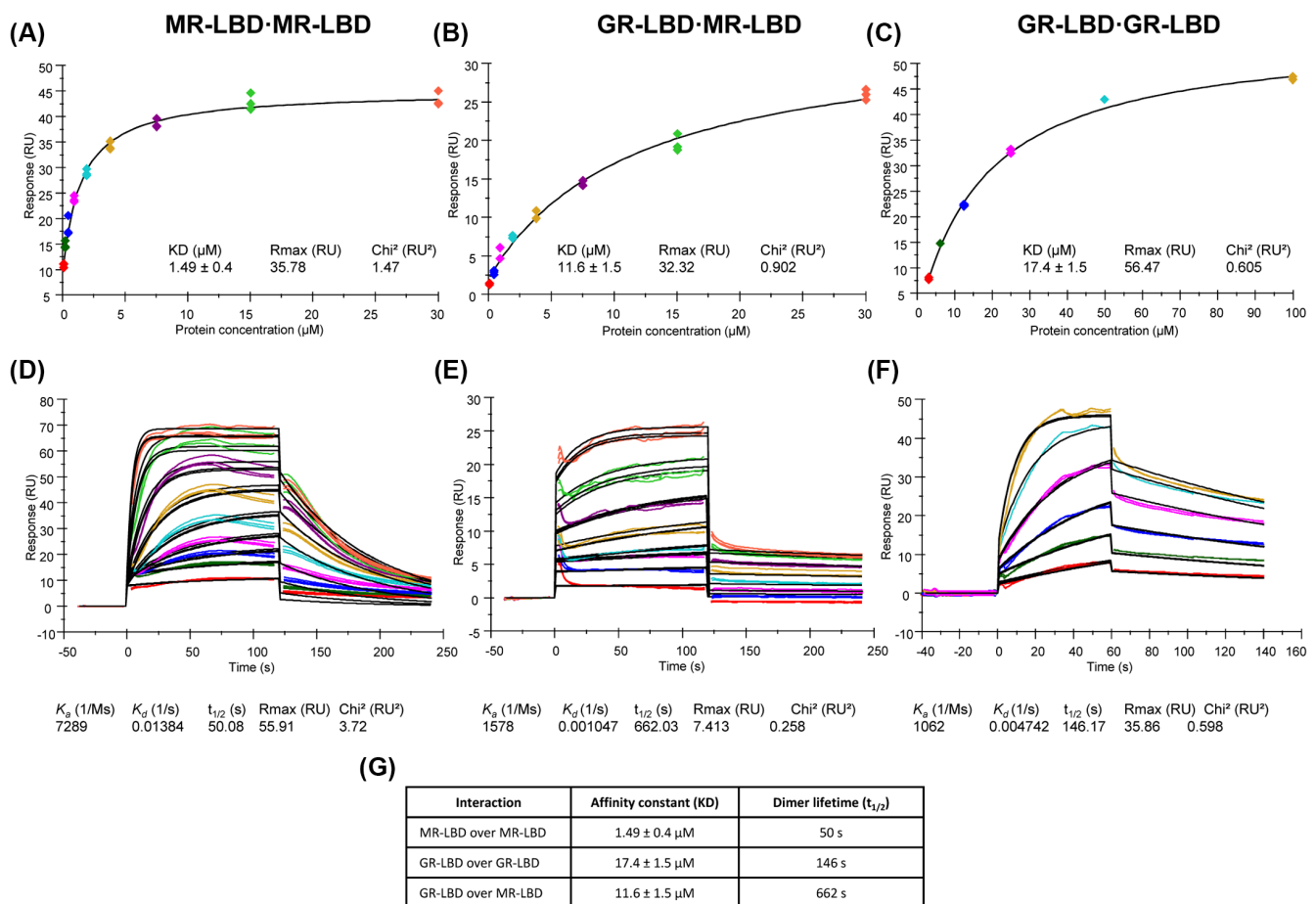


FIGURE 4 Affinity and kinetics of GR- and MR- protein–protein interactions. Surface plasmon resonance (SPR) analysis of either MR-LBD or GR-LBD self-association or heterodimerization were done by (A–C) affinity and (D–F) kinetics. Both immobilized protein and analyte protein run over the immobilized one were expressed and purified in the presence of $50 \mu\text{M}$ Dex. Concentrations specified under the X-axis correspond to the concentration gradient of the analyte protein past over the immobilized protein. Experiments were conducted in triplicates. The table (G) summarizes steady state affinity dissociation constants and complexes half-life.

performed *RNA-seq*. Bioinformatics analyses identified differentially expressed genes (DEGs) with statistical significance in both genotypes (FDR < 0.05) (Table S3). A fold-change plot illustrates Dex versus vehicle gene expression in CO and MR^{EKO} cells (Figure 5A). The overall number of DEGs was almost identical in CO and MR^{EKO} cells (Figure 5B; 457 and 451 DEGs, respectively), with similar percentages of up- and downregulated genes (Figure 5B,C; 70% and 30% vs 64%, and 36%, respectively). Gene expression profiles between CO and MR^{EKO} were very similar, with high overlap between datasets and similar degrees of induction or repression among commonly regulated genes, suggesting a relatively small contribution of MR to the transcriptional response to Dex at this time point in keratinocytes. Upon evaluation of upregulated genes in both genotypes, we found that 16% of CO genes required MR for their regulation, while 8% of genes of the MR^{EKO} dataset were uniquely induced in the absence of this TF (Figure 5C). For downregulated genes, 22% of CO genes were dependent on MR for

regulation, while a striking 33% of MR^{EKO} genes were uniquely repressed, suggesting that MR loss has greater impact on GR-mediated gene repression (Figure 5C).

The expression of selected candidate genes was validated in independent experiments by RT-qPCR. Differences between CO and MR^{EKO} reached statistical significance for genes such as *Tsc22d3/Gilz*, *Per1*, and *Sgk1* (Figure 5D). However, relative gene induction or repression by Dex was of similar magnitude in both genotypes for *Nfil3* and *Dusp10* (Figure 5D).

Functional enrichment analysis by DAVID identified regulation of transcription (23%), apoptosis (14%), T-cell activation (6%), and regulation of hormone secretion (5%) as the most overrepresented processes in Dex upregulated genes common to both genotypes (Figure S4). Most downregulated genes common to both genotypes were involved in signal transduction (60%), regulation of metabolism (43%), regulation of transcription (36%), cell migration (28%), response to stimulus (16%), and T-cell activation (12%), among others (Figure S6).

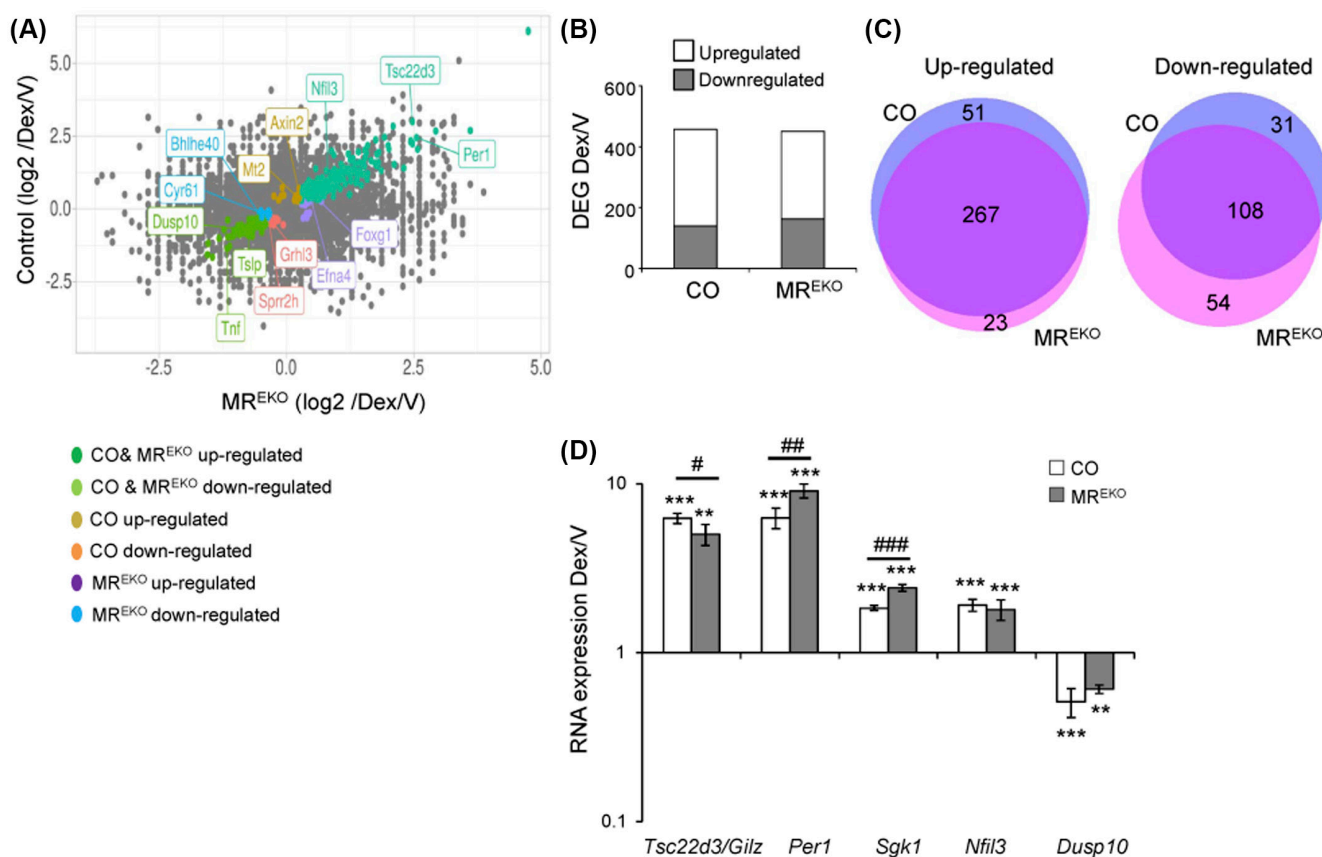


FIGURE 5 Transcriptomic profile in CO and MR^{EKO} keratinocytes upon Dex treatment. (A) Fold-change plot illustrates Dex versus vehicle gene expression *in* CO and MR^{EKO} cells. Differentially expressed genes (DEGs) with statistical significance in both genotypes (FDR < 0.05), up- and downregulated, are highlighted in colors, including examples from indicated categories. (B) Bar graph showing number of DEGs, and (C) Venn diagram indicating overlap between up- and downregulated genes in Dex-treated CO and MR^{EKO} keratinocytes identified by RNA-Seq. (D) Validation of fold-change response (Dex vs vehicle) of the indicated genes in CO and MR^{EKO} keratinocytes by RT-qPCR. Mean values and SD are shown. Statistically significant differences relative to vehicle are denoted by asterisks and those between genotypes by hash symbols ($n = 3-6$; # $p < .05$; ** $p < .01$; *** $p < .001$).

3.5 | MR modifies the kinetics of Dex-induced GR genomic binding

As GR nuclear/cytoplasmic ratio was significantly reduced in MR^{EKO} versus CO at 30–60 min following Dex treatment (Figure 3C), we performed time-course experiments to evaluate whether the loss of MR altered GR binding kinetics on GRE-containing GBS (Figure 6A). In Dex-treated CO cells, GR recruitment to *Nfil3* genomic sequence was detected at 10 min, and peaked at 30 min. However, in MR^{EKO}, GR binding was less pronounced and lagged behind CO only peaking 1 h after Dex (Figure 6A). When we assessed the time-course of *Nfil3* expression in MR^{EKO} versus CO, we found that transcript levels overall paralleled GR-binding kinetics; however, expression was similar in CO and MR^{EKO} 3 h after Dex treatment (Figure 6B).

GR binding to *Nr3c1* and *Dusp10* regulatory sequences followed similar early kinetics in CO and was dramatically decreased in MR-deficient cells (Figure 6A). The lack of GR binding to *Nr3c1* was particularly relevant as it is well known that GR mediates homologous downregulation of its own

gene.^{51,52} Importantly, *Nr3c1* repression by Dex occurred only in CO cells that co-express GR and MR (Figure 6B).

On the other hand, and despite marked differences of GR-binding kinetics between genotypes, *Tsc22d3/Gilz* followed similar expression kinetics, with significant differences between genotypes only at later time points (Figure 6B). This apparent discrepancy is likely due to the contribution of multiple GBS in this gene, of which four were common to both genotypes while one was unique for CO and one for MR^{EKO} (Table S2).

We also assessed GR binding to sequences identified uniquely in MR^{EKO} cells such as *Hlf* and *Lmb2*. While in MR^{EKO} cells, Dex induced early GR binding to *Hlf*, which remained high up to 120 min, binding was not significant in CO cells through the time course (Figure S7). The differences in GR binding were less marked for *Lmb2*, however, the extent of GR recruitment and delayed kinetics was decreased in CO cells (Figure S7). Altogether, these data indicate that MR modulates timing of GR genomic binding in keratinocytes in response to Dex. However, Dex did not elicit changes in *Hlf* or *Lmb2* gene expression

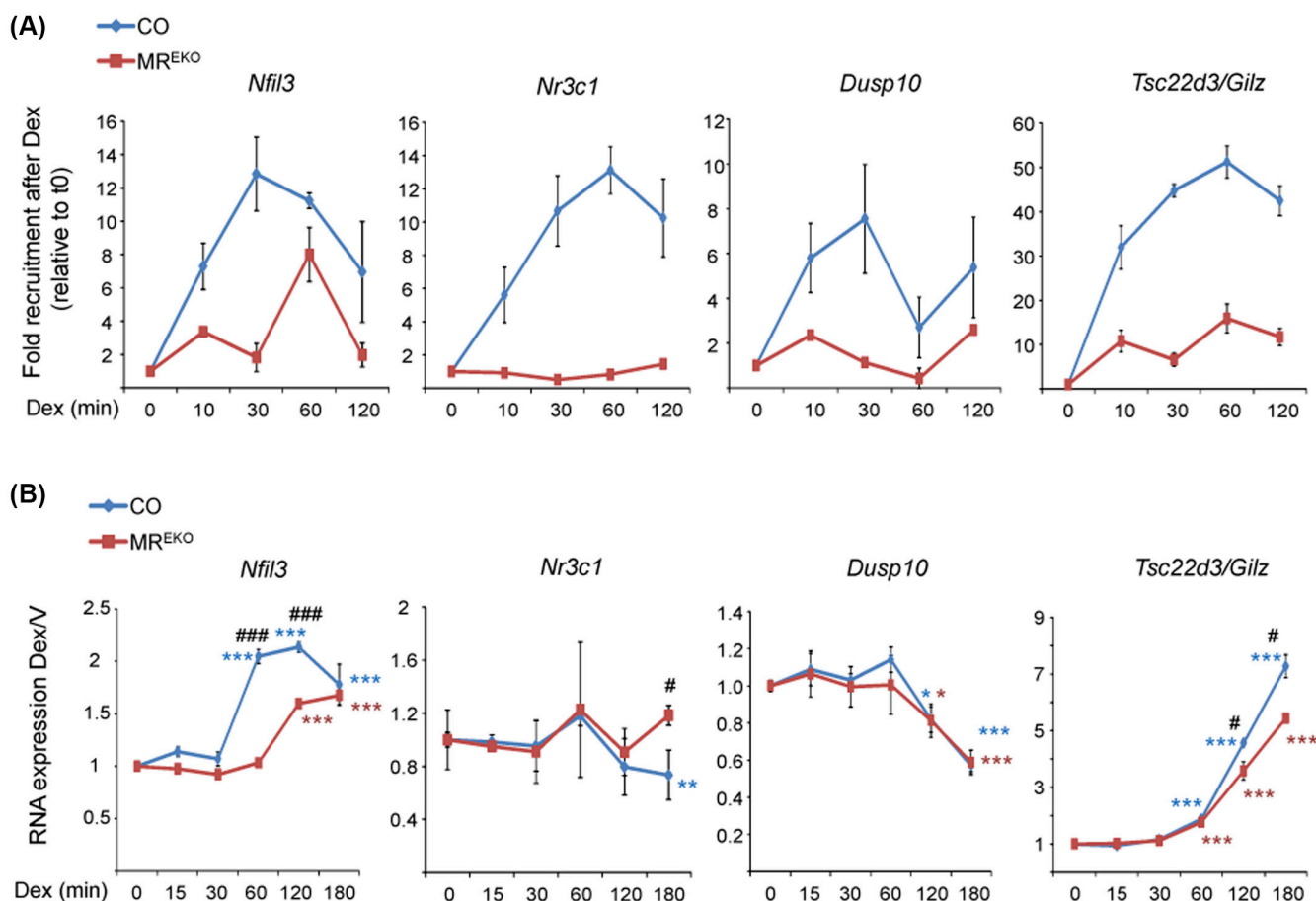


FIGURE 6 MR modifies the kinetics of Dex-induced GR genomic binding and transcriptional regulation. (A) GR ChIP carried out at indicated Dex treatment times to evaluate kinetics of binding to regulatory regions of indicated genes. (B) Dex time-course experiment to determine kinetics of gene expression in CO and MR^{EKO} cells. Mean values and SD are shown. Statistically significant differences relative to vehicle or between genotypes are represented by asterisks or hash symbols, respectively ($n = 3$; *, # $p < .05$; **, ## $p < .01$; ***, ### $p < .001$).

either in the RNA-seq data or the time points assessed (not shown) suggesting that GR binding to these regulatory sequences is unproductive.

Consistent with previous work,⁵⁰ comparison of ChIP-seq and RNA-seq datasets indicated that GR binding showed a higher correlation with gene induction; this was true in both genotypes (Figure S8; 11%–13% of induced genes were bound by GR). Altogether, our data indicate that differences in the magnitude of expression between genotypes upon Dex treatment are gene and time dependent.

4 | DISCUSSION

Our previous work demonstrated the central role of keratinocyte GR in mediating the GC transcriptional response in vitro and in vivo while keratinocyte MR was identified as an important modulator of GR-mediated transcription in this tissue in response to Dex.^{24,30} These data prompted us to address the cell-type specific role of MR in GR genomic binding and transcriptional regulation in response to Dex in keratinocytes by integrated ChIP-seq and RNA-seq analyses.

In this study, we show that the absence of keratinocyte MR correlates with the global reduction of GR genomic binding, and elicits differential GR recruitment to specific TF-binding sites, in particular, a reduction in the number of GREs as well as number of palindromic motifs *per* GBS (Figure 2). Changes in MR^{EKO} versus CO were also in line with a decreased GR nuclear/cytoplasmic ratio (Figure 3D). Even in GRE-containing GBS present in both genotypes, we observed a lower tag count in MR^{EKO} (Figure 2D), suggesting an overall decreased affinity of GR for genomic targets. While these data strongly suggest that Dex induces GR and MR co-binding to DNA, direct proof of concurrent binding is lacking. Also, we cannot rule out that different association patterns of GR in MR^{EKO} versus CO cells after Dex are due to the lack of MR tethering.¹⁶ However, the fact that CORT elicited robust MR binding to GBSs identified by GR ChIP-seq (Figure S3) indicates that distinct receptor–ligand complexes feature different affinities toward regulatory sequences.²³

One major finding is the demonstration of physical complex formation between GR- and MR-LBDs by SPR analyses (Figure 4). The estimated K_D for GR homodimers is similar to previous data on GR and other steroid receptors such as AR and ER.⁵³ Importantly, to the best of our knowledge, this is the first report demonstrating the measurement of MR-LBD self-association affinity and kinetics constants. Indeed, the estimated K_D for MR homodimers was one order of magnitude lower than that obtained for GR homodimer, indicating higher affinity. However,

homodimers of MR had the shortest lifetime, followed by those of GR and GR-MR heterodimers (Figure 4). Taken together, MR-containing dimers showed higher affinity while GR-containing dimers showed the longest lifetime. Therefore, as MR dimers likely represent a minor fraction due to low protein abundance, data indicate that MR mainly acts as modulator of GR-dependent transcription, placing the GR-MR heterodimer—with similar affinity to the GR homodimer but a 4.5-fold longer lifetime—as a key player in response to synthetic GCs.

Our data are also consistent with previous evidence demonstrating that GR-MR interactions can be mediated by alternative interfaces including the GR-LBD.^{15,21} Also, while we demonstrated that GR is able to form oligomers,^{15,53,54} preliminary data indicate that neither MR-MR nor MR-GR form higher order complexes (data not shown).

Collectively, our data not only emphasize the importance of the GR:MR balance in keratinocytes but also support the idea that GR-MR heterodimers represent an important mechanism to extend the regulatory potential of GCs in cells that co-express both receptors.²² Indeed, combinatorial possibilities of GR-MR dimers likely contribute to cooperative or inhibitory transcriptional effects after Dex treatment. The fact that MR loss results in decreased (*Tsc22d3/Gilz*) or increased (*Per1* and *Sgk1*) gene expression (Figure 5C) is consistent with previous reports of MR as a cooperative or antagonistic partner for GR in the GC-dependent transcription.^{16,19,30} It seems feasible that in pathological settings with altered GR:MR ratios, the formation of dimers may shift toward alternative complexes and result in changes in gene expression. This is in line with previous work demonstrating that MR inactivation in skin by genetic and pharmacological approaches reduced the GC-associated side effects in conditions of GC excess in mice and human.^{36,55–57} Also, the fact that MR/*NR3C2* mRNA levels were decreased in human psoriatic lesions⁵⁸ highlights the importance of assessing the response of GR to synthetic GCs in face of the loss-of-function of endogenous MR.

The GR cistrome is cell-type specific and dynamic.⁵⁹ The mechanisms of GR genomic cooperation include its binding as distinct GR and/or GR-MR oligomers, and/or coordinated and synergistic GR-binding events with members of several TF family members including AP-1, C/EBP, STAT, NF- κ B, TEAD, or p53.^{60,61}

The top overrepresented motifs, common to CO and MR^{EKO} keratinocytes, were AP-1, GRE, TEAD, and p53 (Figure 2). It is well known that AP-1 has important roles in regulating gene expression during keratinocyte differentiation, consistent with differential expression of AP-1 family members in specific epidermal layers.^{62,63} However, while AP-1 motifs showed the highest rate of

co-occurrence with GRE motifs in both CO and MR^{EKO} cells, bioinformatic analyses did not identify statistical differences between genotypes (Figure 2). It is feasible that the expression of distinct AP-1 family members has differential effects on the GR- and MR-mediated actions, as reported in HEK293 cells overexpressing these receptors.⁶⁴

Enrichment analyses identified significant differences between TEAD (21% vs 42%) and p53 (7.5% vs 16%) motifs in CO and MR^{EKO} keratinocytes, respectively (Figure 2). The lack of detection of protein–protein interactions between GR and indicated TFs may be due to the experimental conditions used. In addition, there was higher co-occurrence of p53 and other TF motifs at GRE-containing GBS in MR^{EKO} versus CO cells (Figure 2F; 12% vs 6%, respectively), likely due to constitutive increased levels of p63 in MR^{EKO} keratinocytes (Figure 3A,B). We also identified additional TF motifs for STAT, KLF, and NF-1, although overrepresentation was not significant likely due to the restricted cut-off used (data not shown).

Despite the changes in GR genomic binding in MR^{EKO} relative to CO, the transcriptional profiles of both cells upon Dex treatment showed a high overlap (Figure 5 and Figure S5). Nonetheless, several known GC targets with important roles in keratinocytes were differentially expressed upon Dex treatment only in CO cells, including *Krt6a*, *Foxp1*, *Mt1*, *Mt2*, *Cxcl1*, *Spre2*, *Axin2*, *Grhl3*, and *Spr2h*. This is likely due to the basal differences in the transcriptomic profile of MR^{EKO} versus CO keratinocytes, with overrepresentation of keratinocyte differentiation process, including p63 targets such as small proline-rich repeat (*Spr2*) genes (data not shown). This is also consistent with more differentiated status of MR-deficient keratinocytes in vivo as shown by patches of increased keratinization in the epidermis of MR^{EKO} relative to CO mice.³⁶

The choice of time points to perform ChIP-seq and RNA-seq (1 h vs 3 h) was based on previous analyses that showed optimal binding and gene expression changes at these time points.³⁸ However, genomic data showed poor association between these two parameters in both genotypes (Figure S5), consistent with previous reports in other cell types. This may be also due to the fact that binding of MR and GR to specific genomic sites is cyclic, as reported in renal cells.²³ Importantly, time-course experiments showed that gene-dependent differences in the magnitude of expression correlated with earlier and more pronounced GR binding to GRE sites unique to CO, which dramatically decreased in MR-deficient cells (Figure 6; *Nfil3*, *Nr3c1*, and *Dusp10*).

The lack of GR binding to *Nr3c1* in MR^{EKO} cells was particularly relevant as it constitutes, to the best of our

knowledge, the first demonstration that homologous downregulation of *Nr3c1* requires the presence of MR. While in previous work, GC-mediated regulation of GR α mRNA was shown to be mediated through a direct interaction of the receptor with an intragenic nGRE in exon 6 of the gene,⁵¹ here we identified a different genomic site located upstream of the gene (Table S2).

Overall, findings highlight the key role of MR to understand gene- and time-dependent specificity of GC actions, giving support to the combined use of MR antagonists plus GR ligands to improve the therapeutic index—or benefit:risk ratio—of GCs for the treatment of skin inflammatory disorders.^{36,55–57}

AUTHOR CONTRIBUTIONS

Marc Lombès and Paloma Pérez designed the experiments; Elena Carceller-Zazo, Thi An Vu, Géraldine Vitellius, Say Viengchareun, and Yann Jaszczyszyn performed ChIPseq and RNAseq experiments; Elena Carceller-Zazo, Lisa M. Sevilla, and Omar Pons-Alonso performed cell culture work and ChIP-qPCR and RT-qPCR data validation; Elena Carceller-Zazo and Larbi Amazit performed immunofluorescence and high-throughput microscopy; Lisa M. Sevilla performed time-course experiments; Omar Pons-Alonso performed immunoprecipitation and immunoblotting experiments; Álvaro Chiner-Oms and Iñaki Comas performed data processing and bioinformatic analyses; Montserrat Abella, Andrea Alegre-Martí, and Eva Estébanez-Perpiñá did protein expression and purification studies, performed SPR assays, and analyzed data; Lisa M. Sevilla, Omar Pons-Alonso, and Paloma Pérez performed additional bioinformatic analyses; all authors analyzed data and contributed to the discussions; Elena Carceller-Zazo, Lisa M. Sevilla, Omar Pons-Alonso, Andrea Alegre-Martí, Eva Estébanez-Perpiñá, Marc Lombès, and Paloma Pérez contributed to manuscript writing and editing. We affirm that all authors have read and agree with the manuscript.

ACKNOWLEDGMENTS

We thank Mikhail Pachkov from the University of Basel Biozentrum for advice regarding the use of CREMA software. We kindly thank Eric Ortlund (Emory University) for sharing his GR and MR-LBD bacterial expression constructs.

FUNDING INFORMATION

This research is part of the grants PID2020-114652RB-I00 funded by MCIN/AEI/ 10.13039/501100011033 to PP, and PDC2021-121688-I00 to EE-P. The author's work was also supported by Inserm, Université Paris-Saclay. EC-Z was recipient of a postdoctoral fellowship from

the Alfonso Martín Escudero Foundation (Spain); OP-A was funded by EDGJID/2021/098 (Generalitat Valenciana) and by ‘ESF Investing in your future.’. We thank NuRCaMeIN (SAF2017-90604-REDT) for support for dissemination. PP is a member of the Scientific Network on ‘Strategies for therapeutic targeting of the Aldosterone-Mineralocorticoid Receptor signaling pathway (ADMIRE network) funded by the German Research Foundation (DFG-ID 470188766). This work has benefited from the facilities and expertise of the high-throughput sequencing core facility of I2BC (Centre de Recherche de Gif – <http://www.i2bc.paris-saclay.fr/>). This work was supported by the DIM Thérapie Génique Paris Ile-de-France Région, IBISA, and the Labex GR-Ex.

DISCLOSURES

The authors on the manuscript do not have any conflict of interest (either financial or personal).

DATA AVAILABILITY STATEMENT

Project sequencing data are publicly accessible at ENA-EBI under accession number PRJEB54880. Accession numbers for each sample can be found on Table S4.

ORCID

Paloma Pérez  <https://orcid.org/0000-0002-7166-2824>

REFERENCES

- Schäcke H, Döcke WD, Asadullah K. Mechanisms involved in the side effects of glucocorticoids. *Pharmacol Ther.* 2002;96:23-43.
- Vandewalle J, Luypaert A, De Bosscher K, Libert C. Therapeutic mechanisms of glucocorticoids. *Trends Endocrinol Metab.* 2018;29:42-54. doi:10.1016/j.tem.2017.10.010
- Desmet SJ, De BK. Glucocorticoid receptors: finding the middle ground. *J Clin Invest.* 2017;127:1136-1145. doi:10.1172/JCI88886
- Menter A, Korman NJ, Elmetts CA, et al. Guidelines of care for the management of psoriasis and psoriatic arthritis. Section 3. Guidelines of care for the management and treatment of psoriasis with topical therapies. *J Am Acad Dermatol.* 2009;60:643-659. doi:10.1016/j.jaad.2008.12.032
- Timmermans S, Souffriau J, Libert C. A general introduction to glucocorticoid biology. *Front Immunol.* 2019;10:1545. doi:10.3389/FIMMU.2019.01545
- Quax RA, Manenschijn L, Koper JW, et al. Glucocorticoid sensitivity in health and disease. *Nat Rev Endocrinol.* 2013;9:670-686. doi:10.1038/NRENDO.2013.183
- Sacta MA, Chinenov Y, Rogatsky I. Glucocorticoid signaling: an update from a genomic perspective. *Annu Rev Physiol.* 2016;78:155-180. doi:10.1146/annurev-physiol-021115-105323
- Gomez-Sanchez E, Gomez-Sanchez CE. The multifaceted mineralocorticoid receptor. *Compr Physiol.* 2014;4:965-994. doi:10.1002/CPHY.C130044
- De Bosscher K, Desmet SJ, Clarisse D, Estébanez-Perpiña E, Brunsveld L. Nuclear receptor crosstalk - defining the mechanisms for therapeutic innovation. *Nat Rev Endocrinol.* 2020;16:363-377. doi:10.1038/S41574-020-0349-5
- Escoter-Torres L, Greulich F, Quagliarini F, Wierer M, Uhlenhaut NH. Anti-inflammatory functions of the glucocorticoid receptor require DNA binding. *Nucleic Acids Res.* 2020;48:8393-8407. doi:10.1093/nar/gkaa565
- Weikum ER, Knuesel MT, Ortlund EA, Yamamoto KR. Glucocorticoid receptor control of transcription: precision and plasticity via allostery. *Nat Rev Mol Cell Biol.* 2017;18:159-174. doi:10.1038/nrm.2016.152
- Le Billan F, Khan JA, Lamribet K, et al. Cistrome of the aldosterone-activated mineralocorticoid receptor in human renal cells. *FASEB J.* 2015;29:3977-3989. doi:10.1096/FJ.15-274266
- Surjit M, Ganti KP, Mukherji A, et al. Widespread negative response elements mediate direct repression by agonist-Liganded glucocorticoid receptor. *Cell.* 2011;145:224-241. doi:10.1016/J.CELL.2011.03.027
- Jaisser F, Farman N. Emerging roles of the mineralocorticoid receptor in pathology: toward new paradigms in clinical pharmacology. *Pharmacol Rev.* 2016;68:49-75. doi:10.1124/pr.115.011106
- Pooley JR, Rivers CA, Kilcooley MT, et al. Beyond the heterodimer model for mineralocorticoid and glucocorticoid receptor interactions in nuclei and at DNA. *PLoS One.* 2020;15:e0227520.
- Rivers CA, Rogers MF, Stubbs FE, Conway-Campbell BL, Lightman SL, Pooley JR. Glucocorticoid receptor-tethered mineralocorticoid receptors increase glucocorticoid-induced transcriptional responses. *Endocrinology.* 2019;160:1044-1056. doi:10.1210/EN.2018-00819
- Joëls M, De Kloet ER. Coordinative mineralocorticoid and glucocorticoid receptor-mediated control of responses to serotonin in rat hippocampus. *Neuroendocrinology.* 1992;55:344-350. doi:10.1159/000126135
- Trapp T, Rupperecht R, Castren M, Reul JM, Holsboer F. Heterodimerization between mineralocorticoid and glucocorticoid receptor: a new principle of glucocorticoid action in the CNS. *Neuron.* 1994;13:1457-1462. doi:10.1016/0896-6273(94)90431-6
- Liu W, Wang J, Sauter NK, Pearce D. Steroid receptor heterodimerization demonstrated in vitro and in vivo. *Proc Natl Acad Sci U S A.* 1995;92:12480-12484. doi:10.1073/PNAS.92.26.12480
- Ou XM, Storrington JM, Kushwaha N, Albert PR. Heterodimerization of mineralocorticoid and glucocorticoid receptors at a novel negative response element of the 5-HT1A receptor gene. *J Biol Chem.* 2001;276:14299-14307. doi:10.1074/JBC.M005363200
- Savory JGA, Préfontaine GG, Lamprecht C, et al. Glucocorticoid receptor homodimers and glucocorticoid-mineralocorticoid receptor heterodimers form in the cytoplasm through alternative dimerization interfaces. *Mol Cell Biol.* 2001;21:781-793. doi:10.1128/MCB.21.3.781-793.2001
- Koning ASCAM, Buurstede JC, Van Weert LTCM, Meijer OC. Glucocorticoid and mineralocorticoid receptors in the brain: a transcriptional perspective. *J Endocr Soc.* 2019;3:1917-1930. doi:10.1210/JS.2019-00158
- Le Billan F, Amazit L, Bleakley K, et al. Corticosteroid receptors adopt distinct cyclical transcriptional signatures. *FASEB J.* 2018;32:5626-5639. doi:10.1096/FJ.201800391RR

24. Bigas J, Sevilla LM, Carceller E, Boix J, Pérez P. Epidermal glucocorticoid and mineralocorticoid receptors act cooperatively to regulate epidermal development and counteract skin inflammation article. *Cell Death Dis.* 2018;9:588-601. doi:10.1038/s41419-018-0673-z
25. Mifsud KR, Reul JM. Acute stress enhances heterodimerization and binding of corticosteroid receptors at glucocorticoid target genes in the hippocampus. *Proc Natl Acad Sci U S A.* 2016;113:11336-11341. doi:10.1073/PNAS.1605246113/-/DCSUPPLEMENTAL
26. Nishi M, Tanaka M, Matsuda KI, Sunaguchi M, Kawata M. Visualization of glucocorticoid receptor and mineralocorticoid receptor interactions in living cells with GFP-based fluorescence resonance energy transfer. *J Neurosci.* 2004;24:4918-4927. doi:10.1523/JNEUROSCI.5495-03.2004
27. Cato ACB, Weinmann J. Mineralocorticoid regulation of transcription of transfected mouse mammary tumor virus DNA in cultured kidney cells. *J Cell Biol.* 1988;106:2119-2125. doi:10.1083/JCB.106.6.2119
28. Gomez-Sanchez EP, Venkataraman MT, Thwaites D, Fort C. ICV infusion of corticosterone antagonizes ICV-aldosterone hypertension. *Am J Physiol Endocrinol Metab.* 1990;258:E649-E653. doi:10.1152/AJPENDO.1990.258.4.E649
29. Govindan MV, Leclerc S, Roy R, Rathanaswami P, Xie B. Differential regulation of mouse mammary tumor virus-bacterial chloramphenicol acetyltransferase chimeric gene by human mineralocorticoid hormone-receptor complexes. *J Steroid Biochem Mol Biol.* 1991;39:91-103. doi:10.1016/0960-0760(91)90017-Y
30. Sevilla LM, Bigas J, Chiner-Oms Á, Comas I, Sentandreu V, Pérez P. Glucocorticoid-dependent transcription in skin requires epidermal expression of the glucocorticoid receptor and is modulated by the mineralocorticoid receptor. *Sci Rep.* 2020;10:18954. doi:10.1038/s41598-020-75853-5
31. Pooley JR, Flynn BP, Grantved L, et al. Genome-wide identification of basic helix-loop-helix and NF-1 motifs underlying GR binding sites in male rat hippocampus. *Endocrinology.* 2017;158:1486-1501. doi:10.1210/en.2016-1929
32. Watt FM. Mammalian skin cell biology: at the interface between laboratory and clinic. *Science.* 2014;346:937-940. doi:10.1126/SCIENCE.1253734
33. Elias PM, Wakefield JS. Therapeutic implications of a barrier-based pathogenesis of atopic dermatitis. *Clin Rev Allergy Immunol.* 2011;41:282-295. doi:10.1007/S12016-010-8231-1
34. Harris-Tryon TA, Grice EA. Microbiota and maintenance of skin barrier function. *Science.* 2022;376:940-945. doi:10.1126/science.abo0693
35. Sevilla LM, Pérez P. Roles of the glucocorticoid and mineralocorticoid receptors in skin pathophysiology. *Int J Mol Sci.* 2018;19:1906. doi:10.3390/ijms19071906
36. Boix J, Sevilla LM, Sáez Z, Carceller E, Pérez P. Epidermal mineralocorticoid receptor plays beneficial and adverse effects in skin and mediates glucocorticoid responses. *J Invest Dermatol.* 2016;136:2417-2426. doi:10.1016/j.jid.2016.07.018
37. Reichelt J, Haase I. Establishment of spontaneously immortalized keratinocyte lines from wild-type and mutant mice. *Methods Mol Biol.* 2010;585:59-69.
38. Sevilla LM, Latorre V, Carceller E, et al. Glucocorticoid receptor and Klf4 co-regulate anti-inflammatory genes in keratinocytes. *Mol Cell Endocrinol.* 2015;412:281-289. doi:10.1016/j.mce.2015.05.015
39. Heinz S, Benner C, Spann N, et al. Simple combinations of lineage-determining transcription factors prime cis-regulatory elements required for macrophage and B cell identities. *Mol Cell.* 2010;38:576-589. doi:10.1016/J.MOLCEL.2010.05.004
40. Severinova E, Alikunju S, Deng W, Dhawan P, Sayed N, Sayed D. Glucocorticoid receptor-binding and transcriptome signature in Cardiomyocytes. *J Am Heart Assoc.* 2019;8:e011484. doi:10.1161/JAHA.118.011484
41. Robinson JT, Thorvaldsdóttir H, Winckler W, et al. Integrative genomics viewer. *Nat Biotechnol.* 2011;29:24-26. doi:10.1038/nbt.1754
42. Grant CE, Bailey TL. XSTREME: comprehensive motif analysis of biological sequence datasets. *bioRxiv.* 2021;20210902458722. doi:10.1101/2021.09.02.458722
43. Huang DW, Sherman BT, Lempicki RA. Bioinformatics enrichment tools: paths toward the comprehensive functional analysis of large gene lists. *Nucleic Acids Res.* 2009;37:1-13. doi:10.1093/nar/gkn923
44. Huang DW, Sherman BT, Lempicki RA. Systematic and integrative analysis of large gene lists using DAVID bioinformatics resources. *Nat Protoc.* 2009;4:44-57. doi:10.1038/nprot.2008.211
45. Weikum ER, Okafor CD, D'Agostino EH, Colucci JK, Ortlund EA. Structural analysis of the glucocorticoid receptor ligand-binding domain in complex with triamcinolone Acetonide and a fragment of the atypical Coregulator, small heterodimer partner. *Mol Pharmacol.* 2017;92:12-21. doi:10.1124/MOL.117.108506
46. Frank F, Liu X, Ortlund EA. Glucocorticoid receptor condensates link DNA-dependent receptor dimerization and transcriptional transactivation. *Proc Natl Acad Sci U S A.* 2021;118:e2024685118. doi:10.1073/PNAS.2024685118/SUPPL_FILE/PNAS.2024685118.SAPP.PDF
47. Hulsen T, de Vlieg J, Alkema W. BioVenn - a web application for the comparison and visualization of biological lists using area-proportional Venn diagrams. *BMC Genomics.* 2008;9:488. doi:10.1186/1471-2164-9-488
48. Love MI, Huska MR, Jurk M, et al. Role of the chromatin landscape and sequence in determining cell type-specific genomic glucocorticoid receptor binding and gene regulation. *Nucleic Acids Res.* 2017;45:1805-1819. doi:10.1093/nar/gkw1163
49. So AYL, Chaivorapol C, Bolton EC, Li H, Yamamoto KR. Determinants of cell- and gene-specific transcriptional regulation by the glucocorticoid receptor. *PLoS Genet.* 2007;3:927-938. doi:10.1371/journal.pgen.0030094
50. Reddy TE, Pauli F, Sprouse RO, et al. Genomic determination of the glucocorticoid response reveals unexpected mechanisms of gene regulation. *Genome Res.* 2009;19:2163-2171. doi:10.1101/gr.097022.109
51. Ramamoorthy S, Cidlowski JA. Ligand-induced repression of the glucocorticoid receptor gene is mediated by an NCoR1 repression complex formed by long-range chromatin interactions with intragenic glucocorticoid response elements. *Mol Cell Biol.* 2013;33:1711-1722. doi:10.1128/MCB.01151-12
52. Spies LML, Verhoog NJD, Louw A. Acquired glucocorticoid resistance due to homologous glucocorticoid receptor downregulation: a modern look at an age-old problem. *Cell.* 2021;10:2529. doi:10.3390/CELLS10102529
53. Jiménez-Panizo A, Alegre-Martí A, Fettweis G, et al. The multivalency of the glucocorticoid receptor ligand-binding domain

- explains its manifold physiological activities. *Nucleic Acids Res.* 2021;gkac1119. doi:10.1093/nar/gkac1119
54. Presman DM, Ganguly S, Schiltz RL, Johnson TA, Karpova TS, Hager GL. DNA binding triggers tetramerization of the glucocorticoid receptor in live cells. *Proc Natl Acad Sci U S A.* 2016;113:8236-8241. doi:10.1073/pnas.1606774113
 55. Maubec E, Laouénan C, Deschamps L, et al. Topical mineralocorticoid receptor blockade limits glucocorticoid-induced epidermal atrophy in human skin. *J Invest Dermatol.* 2015;135:1781-1789. doi:10.1038/JID.2015.44
 56. Boix J, Nguyen VT, Farman N, Aractingi S, Pérez P. Mineralocorticoid receptor blockade improves glucocorticoid-induced skin atrophy but partially ameliorates anti-inflammatory actions in an irritative model in human skin explants. *Exp Dermatol.* 2018;27:185-187. doi:10.1111/EXD.13473
 57. Perez P. The mineralocorticoid receptor in skin disease. *Br J Pharmacol.* 2022;179:3178-3189. doi:10.1111/bph.15736
 58. Suárez-Fariñas M, Li K, Fuentes-Duculan J, Hayden K, Brodmerkel C, Krueger JG. Expanding the psoriasis disease profile: interrogation of the skin and serum of patients with moderate-to-severe psoriasis. *J Invest Dermatol.* 2012;132:2552-2564. doi:10.1038/JID.2012.184
 59. Escoter-Torres L, Caratti G, Mechtidou A, Tuckermann J, Uhlenhaut NH, Vettorazzi S. Fighting the fire: mechanisms of inflammatory gene regulation by the glucocorticoid receptor. *Front Immunol.* 2019;10:1859. doi:10.3389/FIMMU.2019.01859
 60. Starick SR, Ibn-Salem J, Jurk M, et al. ChIP-exo signal associated with DNA-binding motifs provides insight into the genomic binding of the glucocorticoid receptor and cooperating transcription factors. *Genome Res.* 2015;25:825-835. doi:10.1101/gr.185157.114
 61. Vockley CM, D'Ippolito AM, McDowell IC, et al. Direct GR binding sites potentiate clusters of TF binding across the human genome. *Cell.* 2016;166:1269-1281. doi:10.1016/J.CELL.2016.07.049
 62. Welter JF, Eckert RL. Differential expression of the fos and Jun family members c-fos, fosB, Fra-1, Fra-2, c-jun, junB and junD during human epidermal keratinocyte differentiation. *Oncogene.* 1995;11:2681-2687.
 63. Hanley K, Wood L, Ng DC, et al. Cholesterol sulfate stimulates involucrin transcription in keratinocytes by increasing Fra-1, Fra-2, and Jun D. *J Lipid Res.* 2001;42:390-398. doi:10.1016/S0022-2275(20)31663-1
 64. Dougherty EJ, Elinoff JM, Ferreyra GA, et al. Mineralocorticoid receptor (MR) trans-activation of inflammatory AP-1 signaling: dependence on DNA sequence, MR conformation, and AP-1 family member expression. *J Biol Chem.* 2016;291:23628-23644. doi:10.1074/JBC.M116.732248

SUPPORTING INFORMATION

Additional supporting information can be found online in the Supporting Information section at the end of this article.

How to cite this article: Carceller-Zazo E, Sevilla LM, Pons-Alonso O, et al. The mineralocorticoid receptor modulates timing and location of genomic binding by glucocorticoid receptor in response to synthetic glucocorticoids in keratinocytes. *The FASEB Journal.* 2023;37:e22709. doi:10.1096/fj.202201199RR